AIMS Mathematics

https://www.aimspress.com/journal/Math

AIMS Mathematics, 11(7): 21463–21485.
DOI: 10.3934/math.2026870
Received: 16 April 2026
Revised: 18 June 2026
Accepted: 03 July 2026
Published: 20 July 2026

Research article

Exploring solitary wave solutions of the Drinfeld-Sokolov-Wilson equation

Qinming Yao*

School of Statistics and Data Science, Capital University of Economics and Business, Beijing 100070, China

* **Correspondence:** Email: 32024120101@cueb.edu.cn.

Abstract: Understanding shallow water wave dynamics is essential for coastal engineering, oceanography, and nonlinear physics. In this study, I explored the nonlinear dynamics of the coupled Drinfeld-Sokolov-Wilson system, a key nonlinear partial differential equation model that plays a crucial role in understanding shallow water wave behavior. To investigate the solitary wave solutions of this model, four analytical tools were employed: the Kumar-Malik method, the generalized Arnous method, the Riccati modified extended simple equation method, and the logarithmic transformation. These techniques yielded a variety of soliton solutions, including dark, bright, mixed, kink, bright-dark, breather, multiwave, and mixed-form solitons. Moreover, the periodic, hyperbolic and the exponential function solutions were recovered. This study not only confirms known solutions but significantly enriches the literature on the Drinfeld-Sokolov-Wilson system through the application of novel analytical methods that yield an exceptionally diverse family of soliton solutions, complemented by a comprehensive graphical investigation that illustrates the profound influence of physical parameters on wave dynamics. This study affirms the practical utility of these modern methods while delivering novel insights that advance the theoretical understanding of higher-dimensional wave dynamics.

Keywords: Kumar-Malik method; Riccati modified extended simple equation method; generalized Arnous method; coupled Drinfeld-Sokolov-Wilson; solitons
Mathematics Subject Classification: 35C08, 35Q51

1. Introduction

Understanding complex systems is achievable with nonlinear science and nonlinear partial differential equations (NLPDEs). Chaotic behavior, self-organization, and sensitivity to initial conditions are just some of the emergent behaviors dealing with NLPDEs and nonlinear science [1–3]. NLPDEs have been studied for their soliton wave solutions. Solutions to NLPDEs are essential to understand technical solutions to various nonlinear problems that appear in the engineering and applied sciences. NLPDE models entail many nonlinear processes that appear in the plamsa, fluid, and biological sciences as well as in quantum mechanics [4–7]. NLPDEs, in comparison to numerical methods, provide exact solutions to traveling waves, which enable a deeper understanding of complex nonlinear phenomena in the physical world [8]. NLPDEs are the foundation of nonlinear science which deals with emergent behaviors due to nonlinear interactions, which are the basis of chaotic and nonlinear phenomena [9]. NLPDEs are highly applicable; hence, their study improves our understanding of transitions and bifurcations, as well as the stability of complex systems in various disciplines like science, economics, and engineering [10, 11].

Because of their stability and resemblance to particles, soliton solutions are important to many fields, including pure and applied mathematics, as well as mathematical physics. Given their ability to maintain their shape and energy even when perturbed, they are useful in analyzing wave propagation and studying nonlinear effects in fields such as plasma, fiber optic, and shallow water. They are also relevant to nonlinear differential equations and symmetry as well as integrable systems, and studying solitons helps develop more advanced mathematical models. NLPDEs are the primary means of implementing soliton propagation across the stable and localized nature of any of the sciences [12]. Moreover, the theoretical significance of solitons outside abstract mathematics is demonstrated by practical uses in optical communications where solitons enable the transmission of data with few losses and in plasma physics where solitons are used to understand the processes of fusion. Moreover, there is a great variety of technologies that use solitons, such as controllers, sensors, optical coupling devices, and magneto-optic waveguide structures [13–15]. Solitons have attracted the attention of scientists in many different fields because their possible applications are numerous [16–18].

By exploring solutions to a broad variety of physical processes, one can gain a better insight into the physical behavior at a more fundamental level. The proposed models that will be the core of this context are the NLPDEs because they can be used to inform upcoming research. To have precise solutions, it is necessary to formulate the dynamics of a physical system as an ordinary differential equation or a partial differential equation (PDE). The mathematical modeling of complex natural and industrial processes requires the use of PDEs. As a result, several scholars have come up with different strategies to combat these problems. Several methods have been widely used throughout time: the Adomian decomposition technique [19], improved generalized exponential rational function technique [20], truncated Painlevé technique [21], sensitivity analysis [22], the Riccati equation mapping method [23], Bernoulli (G'/G)-expansion method [24], Darboux transformation [25], (G'/G)-expansion method [26], bifurcation analysis [27], and modified Sardar sub-equation method [28]. Many of the existing analytical methods suffer from certain common limitations, such as heavy computational burden, restricted domain of applicability, strong integrability requirements, and limited ability to produce diverse families of exact solutions.

In this paper, I discuss the dynamics of the coupled Drinfeld-Sokolov-Wilson (DSW) system as important to nonlinear science. The proposed model is a NLPDE system that depicts the interaction of two wave fields between each other. It is used extensively in nonlinear optics, plasma physics, and fluid dynamics, and includes complex wave phenomena such as solitons, kinks, and periodic patterns as a product of nonlinear and dispersive effects.

In this work, I apply advanced integration approaches to derive a variety of soliton solutions, specifically the Kumar-Malik method [29], the generalized Arnous approach [30], the Riccati modified extended simple equation method (RMESEM) [31], and logarithmic transformation analysis [32]. The Kumar-Malik technique is efficient in discovering diverse new soliton solutions. It reduces recursive calculations and lowers the algebraic complexity. Compared to different techniques, this one offers easy calculations and closed-form solutions. The generalized Arnous technique is a helpful method when dealing with higher-order nonlinearities. This method is flexible and general, offering versatile solution forms. The RMESEM is better than the simple equation method in diversifying the range of solutions, including traveling wave solutions. It relies on auxiliary Riccati equations, and, hence, it offers a better range of parameter control. A logarithmic transformation gives the potential to derive a wide range of solutions, including multi-wave solutions, homoclinic breathers, mixed solutions, and periodic solutions. It also helps to provide solutions for more complex interaction types compared to older transformation methods that are too simple and struggle to find these types of solutions. Collectively, these four methods demonstrate distinct advantages over existing approaches by delivering richer and more diverse families of exact solutions, achieving higher computational efficiency, minimizing algebraic complexity, ensuring broader applicability to a wide range of nonlinear models, and providing more systematic procedures for uncovering previously unknown solution structures. The results prove the flexibility and usefulness of such techniques, as effective instruments with significant implications in the engineering and scientific fields. Furthermore, the techniques that have been used have not only enhanced our knowledge on the nonlinear dynamics, but have also provided practical solutions. Mathematical scientists consider these methods very useful because of their flexibility, since they can give more insights and provide new perspectives of exploration and development in nonlinear systems.

The subsequent sections of the article are delineated as follows: In Section 2, I delineate the governing mathematical model. Soliton solutions are derived in Section 3 by using the Kumar-Malik methodology, the RMESEM, and the generalized Arnous method as well as the graphical representations and application. In Section 4, I delineate the interaction phenomena of the proposed model. Conclusions are outlined in Section 5.

2. The governing equation

The DSW equation was first proposed in 1981 by Drinfel'd and Sokolov [33] and Wilson [34] for the dispersive water wave. The wave phenomena derived from this equation are significant in the fields of fluid dynamics, ocean engineering, and science. The successful examination of integrable nonlinear systems has led to many theoretical and practical developments. Integrating mathematical frameworks helps us better understand nonlinear dynamics since they provide insight into important challenges in many fields. The only way to comprehend the intricate physical consequences of nonlinear mathematical problems is to solve them analytically in nonlinear physics. In this work, we study DSW [35–38], read as

$$\begin{cases} U_t + aVV_x = 0, \\ V_t + bUV_x + cU_xV + dV_{xxx} = 0, \end{cases} \tag{2.1}$$

where $U = U(x,t)$ and $V = V(x,t)$ represent wave amplitudes and are functions of space x and time t. The parameters a, b, c, and d are nonzero constants, where b and c are particularly essential to maintain nonlinear coupling; otherwise the system reduces to linear equations. Specifically, a controls the strength of the nonlinear interaction between the two wave fields; b and c characterize the nonlinear coupling and the coupled convection; and d is the dispersion coefficient associated with wave spreading. The system proposed here is aimed at modeling nonlinear wave interactions in shallow water, plasma, and optical media, and captures the combined effects of nonlinearity, dispersion, and inter-field coupling. However, in the literature, the proposed model entails soliton solutions using various techniques. In [35], soliton solutions of the suggested model are investigated by employing the modified extended direct algebraic method. Similarly, in [36], a new auxiliary equation method is applied to study multiple soliton solutions of Eq (2.1). Moreover, the researchers in [37] developed a new generalized (G'/G)-expansion method and those in [38] developed a novel extended direct algebraic method, and both methods are applied for the investigation of the proposed model. To determine different soliton solutions to the proposed model, I delve into the use of sophisticated analytical methods and interaction phenomena.

3. Extraction of solutions

Equation (2.1) can be investigated by employing the transformation delineated by

$$U = U(x,t) = \Psi(\zeta), \quad V = V(x,t) = \Phi(\zeta), \quad \zeta = r(x - st), \tag{3.1}$$

where r and s are arbitrary real constants. Applying the previously described transformations to Eq (2.1), we obtain

$$ar\Phi(\zeta)\Phi'(\zeta) - rs\Psi'(\zeta) = 0, \tag{3.2}$$

$$br\Psi(\zeta)\Phi'(\zeta) + cr\Phi(\zeta)\Psi'(\zeta) + dr^3\Phi^{(3)}(\zeta) - rs\Phi'(\zeta) = 0. \tag{3.3}$$

Integrating Eq (3.2) with zero integration constant results in

$$\frac{1}{2}ar\Phi(\zeta)^2 - rs\Psi(\zeta) = 0, \tag{3.4}$$

where

$$\Psi(\zeta) = \frac{a\Phi(\zeta)^2}{2s}. \tag{3.5}$$

Inserting Eqs (3.5) and (3.2) into Eq (3.3) and then integrating with zero integration constant, we have

$$a(b + 2c)\Phi(\zeta)^3 + 6r^2sd\Phi''(\zeta) - 6s^2\Phi(\zeta) = 0. \tag{3.6}$$

The constant of integration equals zero because localized solitary wave solutions decay and flatten out as we move away from the wave center. Thus, these solutions require the wave profile and the slope to be zero at infinity, which naturally eliminates the constant of integration. A nonzero value would introduce a constant background and would not enable the solution to decay to zero as we move away from the center, thereby creating a wave profile that does not flatten out and is inconsistent with the localized solitary wave behavior that is our focus. Since our primary focus is on solitary wave behavior in shallow water, the constant of integration equals zero for the described solutions from mathematical and a physical perspectives. Consequently, when the principle of homogeneous balancing is applied to the terms $\Phi''(\zeta)$ and $\Phi^3(\zeta)$ in Eq (3.6), then $N = 1$.

3.1. Kumar-Malik method

According to Kumar-Malik [29], the solution for $N = 1$ may be expressed as

$$\Phi(\zeta) = \aleph_0 + \aleph_1\Omega(\zeta), \tag{3.7}$$

with

$$\Omega^{'}(\zeta) = \sqrt{\kappa_1\Omega(\zeta)^4 + \kappa_2\Omega(\zeta)^3 + \kappa_3\Omega(\zeta)^2 + \kappa_4\Omega(\zeta) + \kappa_5}. \tag{3.8}$$

Incorporating (3.7) in conjunction with (3.8) in (3.6), the subsequent solutions are obtained:

Case 1. For $\kappa_5 = \frac{\left(4\kappa_1\kappa_3-\kappa_2^2\right)^2}{64\kappa_1^3}$, $\kappa_4 = \frac{\kappa_2\left(4\kappa_1\kappa_3-\kappa_2^2\right)}{8\kappa_1^2}$ offers $\aleph_1 = \frac{4\kappa_1\aleph_0}{\kappa_2}$, $c = \frac{-3ab\kappa_2^2\aleph_0^2+8ab\kappa_1\kappa_3\aleph_0^2+6\kappa_2^2s^2}{2a\left(3\kappa_2^2-8\kappa_1\kappa_3\right)\aleph_0^2}$, $d = -\frac{8\kappa_1 s}{\left(3\kappa_2^2-8\kappa_1\kappa_3\right)r^2}$. Consequently, the resulting solutions are as follows:

When $\kappa_1 > 0$ and $H = 8\kappa_1\kappa_3 - 3\kappa_2^2 < 0$, we get the kink-type soliton solution

$$V_1(x,t) = -\frac{\sqrt{-H}\aleph_0 \tanh\left(\frac{r\sqrt{-H\kappa_1}(x-st)}{4\kappa_1}\right)}{\kappa_2}, \tag{3.9}$$

and the soliton solution

$$V_2(x,t) = \frac{\sqrt{-H}\aleph_0 \coth\left(\frac{r\sqrt{-H\kappa_1}(x-st)}{4\kappa_1}\right)}{\kappa_2}. \tag{3.10}$$

When $\kappa_1 > 0$ and $H = 8\kappa_1\kappa_3 - 3\kappa_2^2 > 0$, periodic solutions are obtained in the following way:

$$V_3(x,t) = \frac{\sqrt{H}\aleph_0 \tan\left(\frac{r\sqrt{H\kappa_1}(x-st)}{4\kappa_1}\right)}{\kappa_2}, \tag{3.11}$$

$$V_4(x,t) = \frac{\sqrt{H}\aleph_0 \cot\left(\frac{r\sqrt{H\kappa_1}(x-st)}{4\kappa_1}\right)}{\kappa_2}. \tag{3.12}$$

Case 2. For $\kappa_5 = \frac{\kappa_2^2\left(16\kappa_1\kappa_3-5\kappa_2^2\right)}{256\kappa_1^3}$, $\kappa_4 = \frac{\kappa_2\left(4\kappa_1\kappa_3-\kappa_2^2\right)}{8\kappa_1^2}$ offers $\aleph_1 = \frac{4\kappa_1\aleph_0}{\kappa_2}$, $c = \frac{-3ab\kappa_2^2\aleph_0^2+8ab\kappa_1\kappa_3\aleph_0^2+6\kappa_2^2s^2}{2a\left(3\kappa_2^2-8\kappa_1\kappa_3\right)\aleph_0^2}$, $d = -\frac{8\kappa_1 s}{\left(3\kappa_2^2-8\kappa_1\kappa_3\right)r^2}$. So, we get the following:

When $\kappa_1 < 0$ and $H = 8\kappa_1\kappa_3 - 3\kappa_2^2 < 0$, the bright soliton is obtained as follows:

$$V_5(x,t) = \frac{4\kappa_1\aleph_0\left(\frac{\sqrt{-H}\operatorname{sech}\left(\frac{r\sqrt{-H\kappa_1}(x-st)}{2\sqrt{2}\kappa_1}\right)}{2\sqrt{2}\kappa_1} - \frac{\kappa_2}{4\kappa_1}\right)}{\kappa_2} + \aleph_0. \tag{3.13}$$

When $\kappa_1 > 0$ and $H = 8\kappa_1\kappa_3 - 3\kappa_2^2 > 0$, the soliton solution is obtained such as

$$V_6(x,t) = \frac{4\kappa_1\aleph_0\left(\frac{\sqrt{H}\operatorname{csch}\left(\frac{r\sqrt{H\kappa_1}(x-st)}{2\sqrt{2}\kappa_1}\right)}{2\sqrt{2}\kappa_1} - \frac{\kappa_2}{4\kappa_1}\right)}{\kappa_2} + \aleph_0. \tag{3.14}$$

When $\kappa_1 > 0$ and $H = 8\kappa_1\kappa_3 - 3\kappa_2^2 < 0$, the periodic solutions can be recovered as follows:

$$V_7(x,t) = \frac{4\kappa_1\aleph_0\left(\frac{\sqrt{-H}\sec\left(\frac{r\sqrt{-H\kappa_1}(x-st)}{2\sqrt{2}\kappa_1}\right)}{2\sqrt{2}\kappa_1} - \frac{\kappa_2}{4\kappa_1}\right)}{\kappa_2} + \aleph_0, \tag{3.15}$$

$$V_8(x,t) = \frac{4\kappa_1\aleph_0\left(\frac{\sqrt{-H}\csc\left(\frac{r\sqrt{-H\kappa_1}(x-st)}{2\sqrt{2}\kappa_1}\right)}{2\sqrt{2}\kappa_1} - \frac{\kappa_2}{4\kappa_1}\right)}{\kappa_2} + \aleph_0. \tag{3.16}$$

Case 3. For $\kappa_2 = 0$, $\kappa_4 = 0$, $\kappa_5 = 0$ and $\kappa_3 > 0$, offers $\aleph_0 = 0$, $c = \frac{-ab\kappa_3\aleph_1^2 - 12\kappa_1 s^2}{2a\kappa_3\aleph_1^2}$, $d = \frac{s}{\kappa_3 r^2}$. The subsequent solutions are as follows:

$$V_9(x,t) = \frac{4\kappa_3\rho\aleph_1 e^{\sqrt{\kappa_3}r(x-st)}}{4\rho^2 e^{2\sqrt{\kappa_3}r(x-st)} - \kappa_1\kappa_3}. \tag{3.17}$$

By taking $\kappa_1 = -\frac{4\rho^2}{\kappa_3}$ in Eq (3.17), we have

$$V_{10}(x,t) = \frac{\kappa_3\aleph_1 \operatorname{sech}\left(\sqrt{\kappa_3}r(x-st)\right)}{2\rho}. \tag{3.18}$$

Similarly, by taking $\kappa_1 = \frac{4\rho^2}{\kappa_3}$ in Eq (3.17), we have

$$V_{11}(x,t) = \frac{\kappa_3\aleph_1 \operatorname{csch}\left(\sqrt{\kappa_3}r(x-st)\right)}{2\rho}. \tag{3.19}$$

3.1.1. Graphical representations of the obtained solutions with applications

To understand spatiotemporal wave dynamics, three dimensional (3D), two dimensional (2D), and contour graphs are useful. In the field of oceanography, 3D graphs render the amplitude of waves and the geometry of their propagation, 2D graphs show the cross section of the waves and the speed and height of the waves, and the contour maps show the concentration of the energy pertaining to the waves and help predict hazards. In the field of fluid dynamics, these graphs analyze the stability of solitons, phase shifts, and collisions in shallow water or plasma flows. In optical telecommunications, 3D graphs show the intensity of the pulse at a given distance, 2D graphs show the temporal spreading of the pulse, and contour graphs show the nonlinear phase shift of the pulse. The figures have been plotted below for the obtained solutions.

The kink type behavior of solution (3.9) has been sketched in Figure 1 for the parametric values $\kappa_1 = 0.2$, $r = 0.57$, $s = 0.4$, $\aleph_0 = 0.91$, $\kappa_2 = 1.22$ and $\kappa_3 = 0.02$. Kink-type solitons in fluid systems describe sudden changes like a hydraulic jump, a density interface in stratified flows, or a rotating shallow-water interface. The 2D graphs are used to capture the smooth monotonic transition of one equilibrium state to the other, and 3D surfaces to show the time dependence of these step-like waves. Contour plots are useful in mapping how two or more kinks propagate, as well as interact, showing the results of collisions, such as phase shift or annihilation. These graphical tools are useful in enabling engineers to forecast flow instability, mixing layers, and energy dissipation in channels, estuaries, or layers of fluid in the atmosphere.

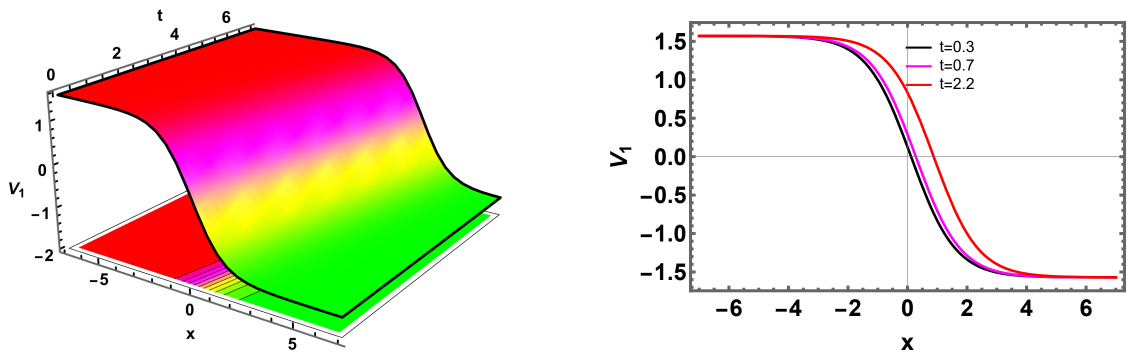

(a) Three dimensional and contour plots **(b)** Two dimensional plot

Figure 1. Plots to solution (3.9).

Figure 2 explains the bright soliton dynamics for solution (3.13) with the assistance of the values such that $\kappa_1 = 0.1$, $r = 0.1$, $s = 0.56$, $\aleph_0 = 2.1$, $\kappa_2 = 5.22$ and $\kappa_3 = 0.01$. Bright solitons in fluid systems are used to model localized elongated high wave packets, like deep-water rogue waves or plasma density pulses, where the 2D graphs have peaked amplitude profiles, and the 3D surfaces depict propagation without dispersion. The contour plots monitor their stability and collisions, which contribute to the prediction of wave hazards. Bright solitons in telecommunication are high-intensity optical pulses in fiber-optic cables, with 2D plots displaying compression or expansion of pulses, 3D surfaces plotting intensity versus distance and time, and contours optimizing the separation of signals to transmit data loosely over long distances.

Moreover, the periodic dynamics for solution (3.15) has been plotted in Figure 3 with the parametric values $\kappa_1 = 0.1$, $r = 0.51$, $s = 3.56$, $\aleph_0 = 0.1$, $\kappa_2 = 2.22$ and $\kappa_3 = 1.01$. The values $\rho = 0.28$, $\kappa_1 = 1.1$, $\kappa_3 = 0.1$, $r = 0.051$, $s = 0.06$ and $\aleph_1 = 0.1$ are used for the dynamical behavior of solution (3.18) in Figure 4.

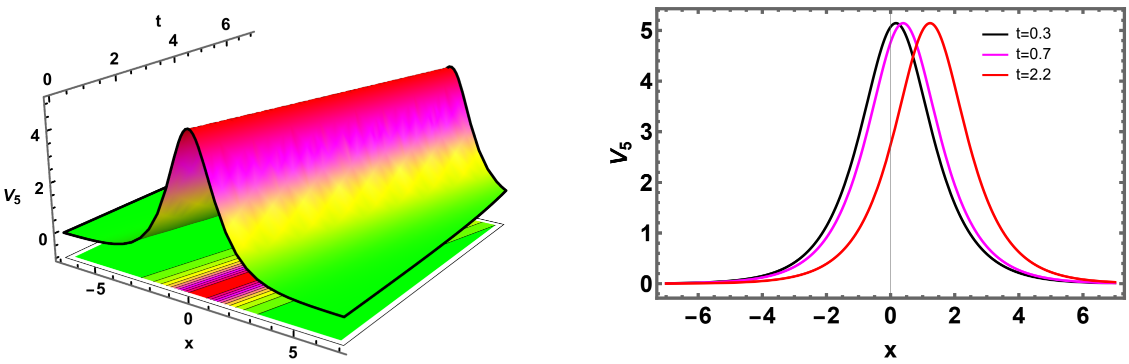

(a) Three dimensional and contour plots **(b)** Two dimensional plot

Figure 2. Plots to solution (3.13).

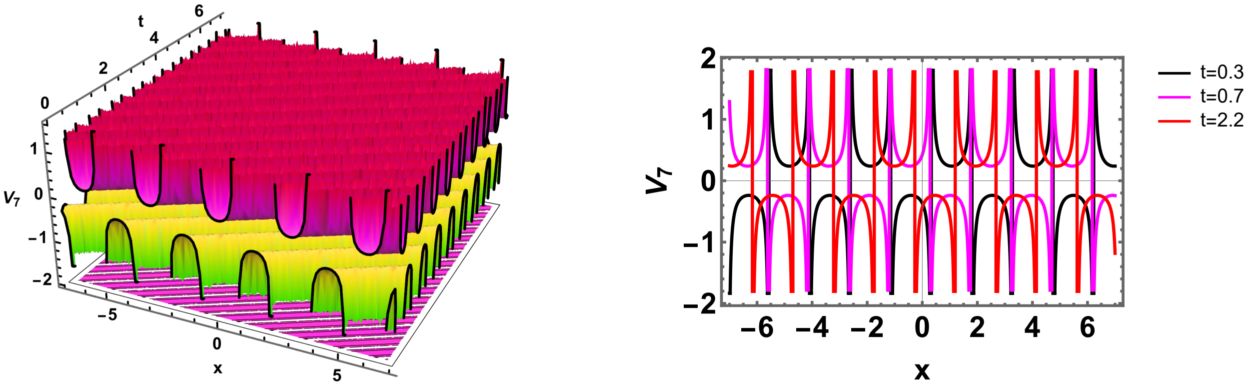

(a) Three dimensional and contour plots **(b)** Two dimensional plot

Figure 3. Plots to solution (3.15).

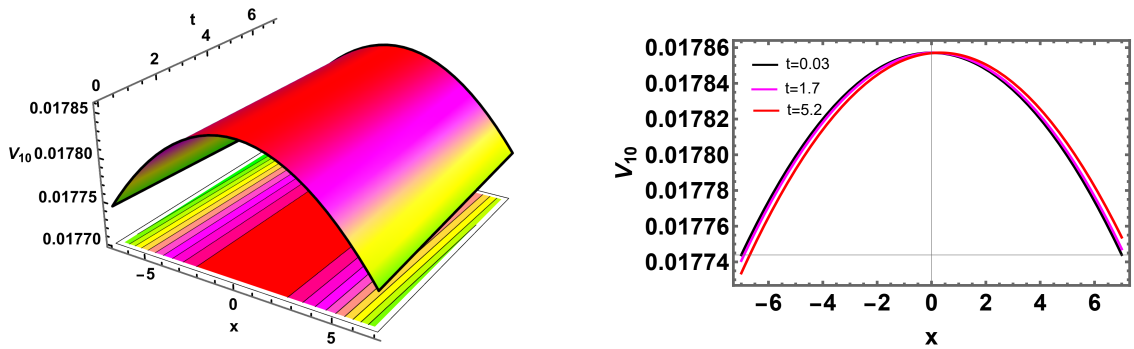

(a) Three dimensional and contour plots **(b)** Two dimensional plot

Figure 4. Plots to solution (3.18).

3.2. Generalized Arnous method

The solution for the generalized Arnous a pproach [30] may be stated as

$$\Phi(\zeta) = \aleph_0 + \sum_{r=1}^{N} \frac{\aleph_r}{(\Theta(\zeta))^r} + \sum_{r=1}^{N} \frac{\kappa_r (\Theta'(\zeta))^r}{(\Theta(\zeta))^r} \tag{3.20}$$

with $N = 1$, and Eq (3.20) is described by

$$\Phi(\zeta) = \aleph_0 + \frac{\aleph_1}{\Theta(\zeta)} + \frac{\kappa_1 \Theta'(\zeta)}{\Theta(\zeta)}, \tag{3.21}$$

where the letters $\aleph_0$, $\aleph_1$, and κ_1 are constants that will be identified later, and the function $\Theta(\zeta)$ is defined by the relation below:

$$(\Theta'(\zeta))^2 = \ln(\delta)^2 \left(\Theta(\zeta)^2 - \rho\right), \tag{3.22}$$

with

$$\Theta^{(n)}(\zeta) = \begin{cases} \Theta'(\zeta)\ln(\delta)^2, & n \text{ is odd,} \\ \Theta(\zeta)\ln(\delta)^2, & n \text{ is even,} \end{cases}$$

for $n \geq 2$, $\delta \neq 1$, and $\delta > 0$. The solution to Eq (3.22) is as follows:

$$\Theta(\zeta) = Q\ln(\delta)\delta^{\zeta} + \frac{\rho}{4Q\ln(\delta)\delta^{\zeta}}, \tag{3.23}$$

where ρ and Q are arbitrarily chosen parameters. When Eq (3.21) is combined with Eq (3.22) in Eq (3.6), the general solutions are as follows:

Set I. When $\aleph_0 = 0$, $\aleph_1 = 0$, $c = \frac{3s^2}{a\kappa_1^2\log^2(\delta)} - \frac{b}{2}$, $d = -\frac{s}{2r^2\log^2(\delta)}$. The required solutions with the calculated data are secured as follows:

$$V_1(x,t) = \frac{a\left(\frac{\kappa_1\log(\delta)\left(4Q^2\log^2(\delta)\delta^{2r(x-st)}-\rho\right)}{\rho+4Q^2\log^2(\delta)\delta^{2r(x-st)}}\right)^2}{2s}. \tag{3.24}$$

With $\rho = 4Q^2$ and $\delta = e$, solution (3.24) is described as follows:

$$V_2(x,t) = \kappa_1\tanh(r(x-st)). \tag{3.25}$$

Similarly, with $\rho = -4Q^2$ and $\delta = e$, solution (3.24) is as follows:

$$V_3(x,t) = \kappa_1\coth(r(x-st)). \tag{3.26}$$

Set II. When $\aleph_0 = 0$, $\aleph_1 = -\frac{2\sqrt{3}\sqrt{\rho}s}{\sqrt{a(b+2c)}}$, $\kappa_1 = 0$, $d = \frac{s}{r^2\log^2(\delta)}$. In accordance with the calculated data, the appropriate solutions are secured as follows:

$$V_4(x,t) = -\frac{8\sqrt{3}\sqrt{\rho}Qs\log(\delta)\delta^{r(x-st)}}{\sqrt{a(b+2c)}\left(\rho+4Q^2\log^2(\delta)\delta^{2r(x-st)}\right)}. \tag{3.27}$$

With $\rho = 4Q^2$ and $\delta = e$, solution (3.27) is described as follows:

$$V_5(x,t) = \frac{2\sqrt{3}\sqrt{Q^2}s\operatorname{sech}(r(x-st))}{Q\sqrt{a(b+2c)}}. \tag{3.28}$$

Similarly, with $\rho = -4Q^2$ and $\delta = e$, solution (3.27) is as follows:

$$V_6(x,t) = -\frac{2\sqrt{3}\sqrt{-Q^2}s\operatorname{csch}(r(x-st))}{Q\sqrt{ab+2ac}}. \tag{3.29}$$

Set III. When $\aleph_0 = 0$, $\aleph_1 = i\kappa_1\sqrt{\rho}\log(\delta)$, $c = \frac{3s^2}{a\kappa_1^2\log^2(\delta)} - \frac{b}{2}$, $d = -\frac{2s}{r^2\log^2(\delta)}$. The required solutions with the calculated data are secured as follows:

$$V_7(x,t) = \frac{\kappa_1\log(\delta)\left(2Q\log(\delta)\delta^{r(x-st)} + i\sqrt{\rho}\right)}{2Q\log(\delta)\delta^{r(x-st)} - i\sqrt{\rho}}. \tag{3.30}$$

With $\rho = 4Q^2$ and $\delta = e$, solution (3.30) is described as follows:

$$V_8(x,t) = \kappa_1(\tanh(r(x-st)) + i\operatorname{sech}(r(x-st))). \tag{3.31}$$

Similarly, with $\rho = -4Q^2$ and $\delta = e$, solution (3.30) is as follows:

$$V_9(x,t) = \kappa_1\coth(r(x-st)) - \kappa_1\operatorname{csch}(r(x-st)). \tag{3.32}$$

3.2.1. Graphical representations of the obtained solutions with applications

Figure 5 offers the dynamics of the solution (3.24) for the parametric values $a = 3.1$, $\delta = 0.3$, $\kappa_1 = 0.28$, $\rho = 0.12$, $Q = 0.1$, $r = 0.06$, and $s = 0.6$.

The 3D graph demonstrates how a value V_1 (between 0.00 and 0.10) varies as you move along space and time in the manner of a wave increasing or decreasing. The contour lines are similar to equal-height marks on a map, and it is easy to observe where V_1 remains the same as it travels along space and time. The 2D graph shows how variable V_1 (from 0.00 to 0.06) changes along the x-axis at three different times. Each curve is a snapshot at a time, which enables one to observe how the shape and height of the signal change as time goes on. These graphs are used in the ocean modeling to track the wave patterns, tsunami propagation, or spread of pollutants in space and time to aid in early warning and coastal management.

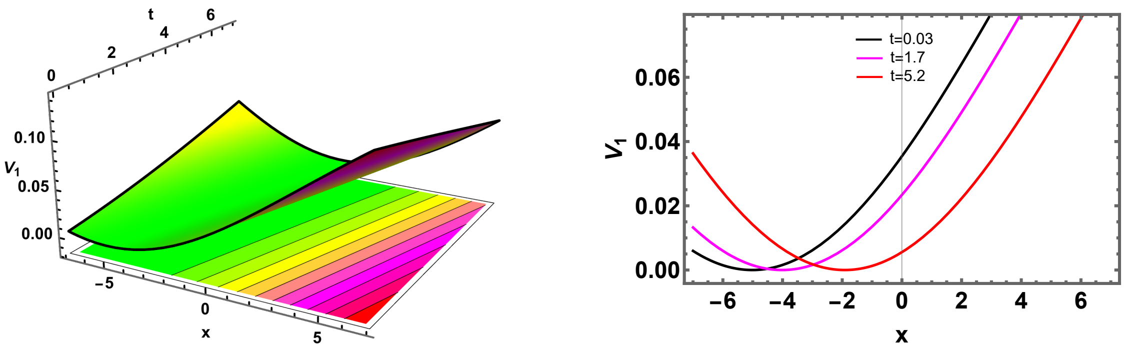

(a) Three dimensional and contour plots

(b) Two dimensional plot

Figure 5. Plots to solution (3.24).

Moreover, Figure 6 is sketched for the parametric values $a = 0.1$, $\delta = 0.3$, $\kappa_1 = 0.028$, $\rho = 3.12$, $Q = 0.1$, $r = 2.06$, and $s = 0.09$ to solution (3.30).

The 3D graph in Figure 6(a) illustrates the dependence of variable (between −0.0005 to 0.005) on space x and time t in case V_7 to create a surface that discloses the spatiotemporal behavior. The 2D graph in Figure 6(b) presents V_7 (between −0.00006 to 0.00006) on the x-axis at three time snapshot, and each curve presents the spatial profile at that point. Combined, they aid in visualizing the evolution of small amplitude signals, be it growth, decay, or propagation, in space and time. The 3D graph in Figure 6(c) shows how the value V_7 changes across space x and time t. The 2D graph in Figure 6(d) shows along the x-axis at three times, with each line showing the shape at that moment. In ocean studies, these graphs can be used to plot the travel distance and time of small variations in water height or pressure, and can help with tsunami warnings and marine safety.

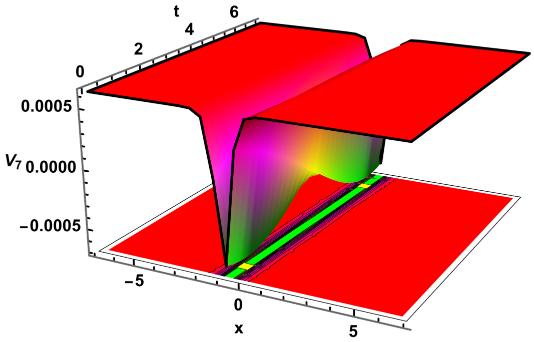

(a) Three dimensional and contour plots (Real part)

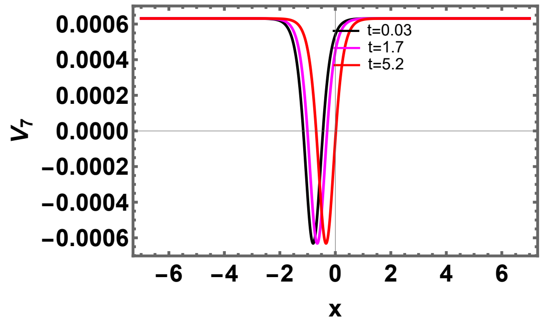

(b) Two dimensional plot (Real part)

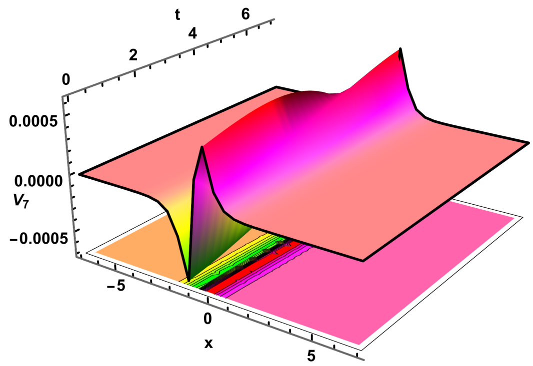

(c) Three dimensional and contour plots (Imaginary part)

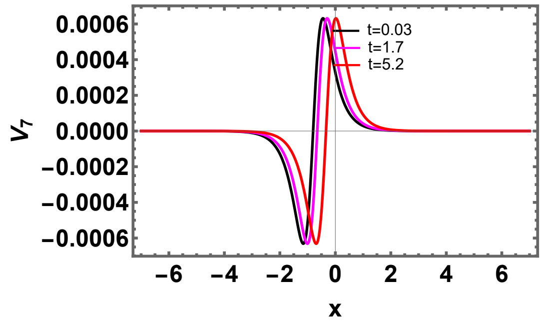

(d) Two dimensional plot (Imaginary part)

Figure 6. Plots to solution (3.30).

3.3. Riccati modified extended simple equation method

The solution of RMESEM [31] is described as

$$\Phi(\zeta) = \sum_{j=0}^{N} \aleph_j \left(\frac{\Omega'(\zeta)}{\Omega(\zeta)}\right)^j + \sum_{\omega=0}^{N-1} \kappa_\omega \left(\frac{\Omega'(\zeta)}{\Omega(\zeta)}\right)^\omega \cdot \left(\frac{1}{\Omega(\zeta)}\right) \quad (\omega = 0, 1, 2, \cdots N-1). \tag{3.33}$$

Taking $N = 1$ in Eq (3.33) results in

$$\Phi(\zeta) = \aleph_0 + \aleph_1 \left(\frac{\Omega'(\zeta)}{\Omega(\zeta)}\right) + \frac{\kappa_0}{\Omega(\zeta)}, \tag{3.34}$$

with $\Omega'(\zeta) = \lambda + \mu\Omega(\zeta) + \nu\Omega(\zeta)^2$.

The incorporation of Eqs (3.33) and (3.34) into Eq (3.6) produces the solutions as follows:

Family 1.

Set 1. For $\aleph_0 = -\frac{1}{2}(\mu\aleph_1)$, $\kappa_0 = -\lambda\aleph_1$, $c = \frac{12s^2}{aG\aleph_1^2} - \frac{b}{2}$, $d = -\frac{2s}{Gr^2}$, $G = \mu^2 - 4\lambda\nu < 0$, we obtain the periodic solution as below:

$$V_1(x,t) = \frac{\aleph_1 \tan\left(\frac{1}{2}\sqrt{-G}r(x-st)\right)\left(\sqrt{-G}\mu + G\tan\left(\frac{1}{2}\sqrt{-G}r(x-st)\right)\right)}{2\left(\mu - \sqrt{-G}\tan\left(\frac{1}{2}\sqrt{-G}r(x-st)\right)\right)}. \tag{3.35}$$

Set 2. When $\aleph_1 = 0,\ \kappa_0 = \frac{2\lambda\aleph_0}{\mu},\ c = \frac{3\mu^2 s^2}{aG\aleph_0^2} - \frac{b}{2},\ d = -\frac{2s}{Gr^2}$, and $G = \mu^2 - 4\lambda\nu < 0$, we obtain the periodic solution such as

$$V_2(x,t) = \aleph_0\left(1 - \frac{4\lambda\nu}{\mu^2 - \sqrt{-G}\mu\tan\left(\frac{1}{2}\sqrt{-G}r(x-st)\right)}\right). \tag{3.36}$$

Family 2.

Set 1. When $\aleph_0 = -\frac{1}{2}\left(\mu\aleph_1\right),\ \kappa_0 = -\lambda\aleph_1,\ c = \frac{12s^2}{aG\aleph_1^2} - \frac{b}{2},\ d = -\frac{2s}{Gr^2}$, and $G = \mu^2 - 4\lambda\nu < 0$, we obtain the following solutions:

$$V_3(x,t) = \frac{\aleph_1\cot\left(\frac{1}{2}\sqrt{-G}r(x-st)\right)\left(G\cot\left(\frac{1}{2}\sqrt{-G}r(x-st)\right) - \sqrt{-G}\mu\right)}{2\left(\sqrt{-G}\cot\left(\frac{1}{2}\sqrt{-G}r(x-st)\right) + \mu\right)}. \tag{3.37}$$

Set 2. When $\aleph_1 = 0,\ \kappa_0 = \frac{2\lambda\aleph_0}{\mu},\ c = \frac{3\mu^2 s^2}{aG\aleph_0^2} - \frac{b}{2},\ d = -\frac{2s}{Gr^2}$, and $G = \mu^2 - 4\lambda\nu < 0$, we have

$$V_4(x,t) = \aleph_0\left(1 - \frac{4\lambda\nu}{\sqrt{-G}\mu\cot\left(\frac{1}{2}\sqrt{-G}r(x-st)\right) + \mu^2}\right). \tag{3.38}$$

Family 3.

Set 1. When $\aleph_0 = -\frac{1}{2}\left(\mu\aleph_1\right),\ \kappa_0 = -\lambda\aleph_1,\ c = \frac{12s^2}{aG\aleph_1^2} - \frac{b}{2},\ d = -\frac{2s}{Gr^2}$, and $G = \mu^2 - 4\lambda\nu < 0$, the periodic solution can be obtained as

$$\begin{aligned} V_5(x,t) = \frac{1}{2}\aleph_1 \Bigg(& \frac{2(-G)\left(\sin\left(\sqrt{-G}r(x-st)\right)+1\right)\sec\left(\sqrt{-G}r(x-st)\right)}{\sqrt{-G}\left(\sin\left(\sqrt{-G}r(x-st)\right)+1\right) - \mu\cos\left(\sqrt{-G}r(x-st)\right)} - \mu \\ & - \frac{4\lambda\nu}{\sqrt{-G}\left(\tan\left(\sqrt{-G}r(x-st)\right) + \sec\left(\sqrt{-G}r(x-st)\right)\right) - \mu}\Bigg). \end{aligned} \tag{3.39}$$

Set 2. When $\aleph_1 = 0,\ \kappa_0 = \frac{2\lambda\aleph_0}{\mu},\ c = \frac{3\mu^2 s^2}{aG\aleph_0^2} - \frac{b}{2},\ d = -\frac{2s}{Gr^2}$, and $G = \mu^2 - 4\lambda\nu < 0$, the following periodic solution can be obtained:

$$V_6(x,t) = \aleph_0\left(\frac{4\lambda\nu}{\mu\left(\sqrt{-G}\left(\tan\left(\sqrt{-G}r(x-st)\right) + \sec\left(\sqrt{-G}r(x-st)\right)\right) - \mu\right)} + 1\right). \tag{3.40}$$

Family 4.

Set 1. When $\aleph_0 = -\frac{1}{2}\left(\mu\aleph_1\right),\ \kappa_0 = -\lambda\aleph_1,\ c = \frac{12s^2}{aG\aleph_1^2} - \frac{b}{2},\ d = -\frac{2s}{Gr^2}$, and $G = \mu^2 - 4\lambda\nu > 0$, the dark soliton is as follows:

$$V_7(x,t) = -\frac{\aleph_1\tanh\left(\frac{1}{2}\sqrt{G}r(x-st)\right)\left(\sqrt{G}\mu + G\tanh\left(\frac{1}{2}\sqrt{G}r(x-st)\right)\right)}{2\left(\sqrt{G}\tanh\left(\frac{1}{2}\sqrt{G}r(x-st)\right) + \mu\right)}. \tag{3.41}$$

Set 2. When $\aleph_1 = 0,\ \kappa_0 = \frac{2\lambda\aleph_0}{\mu},\ c = \frac{3\mu^2 s^2}{aG\aleph_0^2} - \frac{b}{2},\ d = -\frac{2s}{Gr^2}$, and $G = \mu^2 - 4\lambda\nu > 0$, the solution is as follows:

$$V_8(x,t) = \aleph_0\left(1 - \frac{4\lambda\nu}{\sqrt{G}\mu\tanh\left(\frac{1}{2}\sqrt{G}r(x-st)\right) + \mu^2}\right). \tag{3.42}$$

Family 5.

Set 1. When $\aleph_0 = -\frac{1}{2}(\mu\aleph_1),\ \kappa_0 = -\lambda\aleph_1,\ c = \frac{12s^2}{aG\aleph_1^2} - \frac{b}{2},\ d = -\frac{2s}{Gr^2}$, and $G = \mu^2 - 4\lambda\nu > 0$, we obtain the dark soliton solution:

$$\begin{aligned} V_9(x,t) = &-\frac{\mu\aleph_1}{2} - \frac{G\aleph_1\left(-1 + i\sinh\left(\sqrt{G}r(x-st)\right)\right)\operatorname{sech}\left(\sqrt{G}r(x-st)\right)}{\mu\cosh\left(\sqrt{G}r(x-st)\right) + \sqrt{G}\sinh\left(\sqrt{G}r(x-st)\right) + i\sqrt{G}} \\ &- \frac{\lambda\aleph_1}{-\frac{\mu}{2\nu} - \frac{\sqrt{G}\left(\tanh\left(\sqrt{G}r(x-st)\right) + i\operatorname{sech}\left(\sqrt{G}r(x-st)\right)\right)}{2\nu}}. \end{aligned} \tag{3.43}$$

Family 6.

Set 1. When $\aleph_0 = -\frac{1}{2}(\mu\aleph_1),\ \kappa_0 = -\lambda\aleph_1,\ c = \frac{12s^2}{aG\aleph_1^2} - \frac{b}{2},\ d = -\frac{2s}{Gr^2}$, and $G = \mu^2 - 4\lambda\nu > 0$, we get the bright dark solution:

$$\begin{aligned} V_{10}(x,t) = \frac{1}{4}\Bigg(&\frac{8\lambda\nu}{\sqrt{G}\coth\left(\sqrt{G}r(x-st)\right) + \sqrt{G}\operatorname{csch}\left(\sqrt{G}r(x-st)\right) + \mu} \\ &+ \frac{2G\coth\left(\frac{1}{2}\sqrt{G}r(x-st)\right)}{\mu\sinh\left(\frac{1}{2}\sqrt{G}r(x-st)\right) - \sqrt{G}} - 2\mu\Bigg). \end{aligned} \tag{3.44}$$

Set 2. When $\aleph_1 = 0,\ \kappa_0 = \frac{2\lambda\aleph_0}{\mu},\ c = \frac{3\mu^2 s^2}{aG\aleph_0^2} - \frac{b}{2},\ d = -\frac{2s}{Gr^2}$, and $G = \mu^2 - 4\lambda\nu > 0$, we have the combined soliton solution as follows:

$$V_{11}(x,t) = \aleph_0\left(1 - \frac{4\lambda\nu}{\mu\left(\sqrt{G}\coth\left(\sqrt{G}r(x-st)\right) + \sqrt{G}\operatorname{csch}\left(\sqrt{G}r(x-st)\right) + \mu\right)}\right). \tag{3.45}$$

Family 7.

When $\aleph_0 = -\frac{1}{2}(\mu\aleph_1),\ \kappa_0 = 0,\ c = \frac{12s^2}{a\mu^2\aleph_1^2} - \frac{b}{2},\ d = -\frac{2s}{\mu^2 r^2},\ \lambda = 0,\ \mu = \tau$, and $\nu = h\tau$, we get the following solution:

$$V_{12}(x,t) = \frac{\tau\aleph_1\left(h + e^{r\tau(x-st)}\right)}{2\left(e^{r\tau(x-st)} - h\right)}. \tag{3.46}$$

Family 8.

When $\aleph_0 = -\frac{1}{2}(\mu\aleph_1),\ \kappa_0 = 0,\ c = \frac{12s^2}{a\mu^2\aleph_1^2} - \frac{b}{2},\ d = -\frac{2s}{\mu^2 r^2},\ \lambda = 0,\ \mu = \tau$, and $\nu = h\tau$, we get the following solution:

$$V_{13}(x,t) = \frac{1}{2}\tau\aleph_1\left(-\frac{2}{he^{r\tau(x-st)} - 1} - 1\right). \tag{3.47}$$

Family 9.
When $\aleph_0 = -\frac{1}{2}(\mu\aleph_1)$, $\kappa_0 = 0$, $c = \frac{12s^2}{a\mu^2\aleph_1^2} - \frac{b}{2}$, and $d = -\frac{2s}{\mu^2 r^2}$, we get the following soliton solution:

$$V_{14}(x,t) = -\frac{\mu\aleph_1(\rho + \sinh(\mu r(x-st)) - \cosh(\mu r(x-st)))}{2(\rho - \sinh(\mu r(x-st)) + \cosh(\mu r(x-st)))}. \tag{3.48}$$

3.3.1. Graphical representations of the obtained solutions with applications

The kink and dark type dynamics have been observed in Figure 7 for the solution (3.43) by the assistance of the parametric values $\lambda = 1.1$, $\mu = 1.92$, $\nu = 0.83$, $r = 6$, $s = 0.16$, and $\aleph_1 = 0.5$.

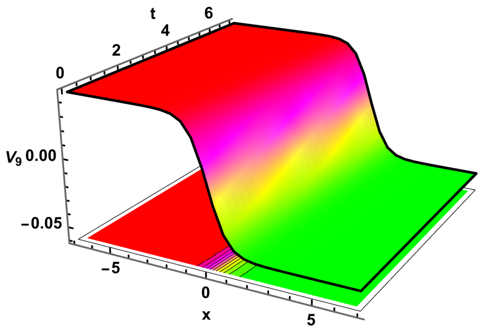

(a) Three dimensional and contour plots (Real part)

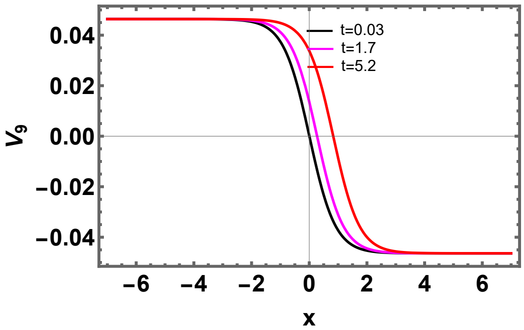

(b) Two dimensional plot (Real part)

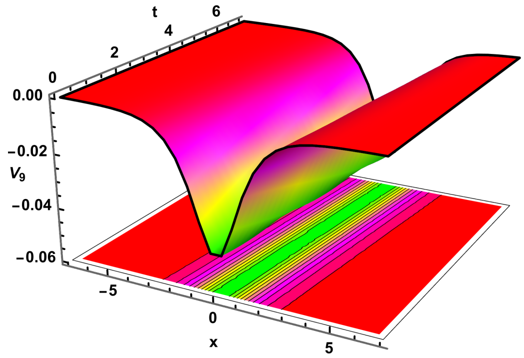

(c) Three dimensional and contour plots (Imaginary part)

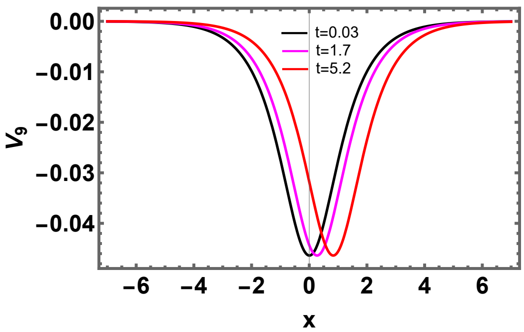

(d) Two dimensional plot (Imaginary part)

Figure 7. Plots to solution (3.43).

In fluid dynamics, kink-type solitons are used to model sharp interface transitions, such as internal waves and bore propagation, enabling the prediction of non-dispersive transport of energy in stratified flows. They are used in telecommunications as powerful binary signal carriers in optical fibers, where their topological robustness reduces distortion and enables high-speed and long-range transmission of data over long distances. Their shape stability under nonlinear and dispersive influence guarantees their reliability in signal integrity of the hydrodynamic waveguide and photonic waveguide. Therefore, kink solitons solve the gap between theoretical nonlinear physics and real-world engineering to improve efficiency and stability of fluid management and worldwide communication infrastructure.

Moreover, Figure 8 has been sketched to explain the dynamics of the solution (3.48) with the parametric values $\mu = 3.2i$, $\rho = 2.0092$, $r = 0.66$, $s = 0.06$, and $\aleph_1 = 2.5$.

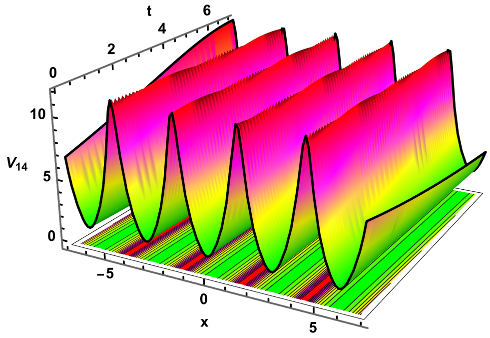

(a) Three dimensional and contour plots (Absolute)

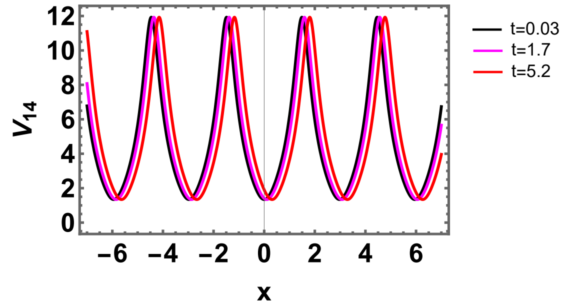

(b) Two dimensional plot (Absolute part)

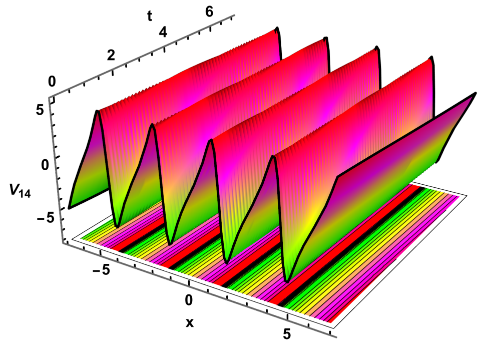

(c) Three dimensional and contour plots (Real part)

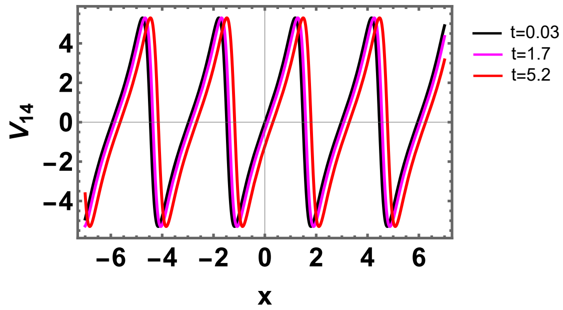

(d) Two dimensional plot (Real part)

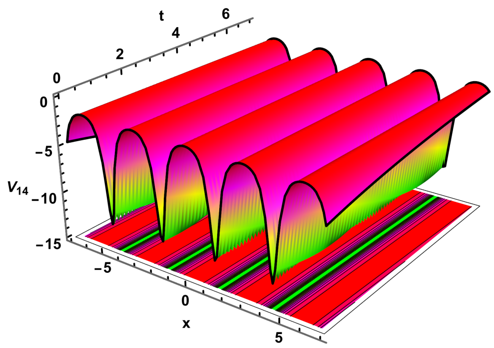

(e) Three dimensional and contour plots (Imaginary part)

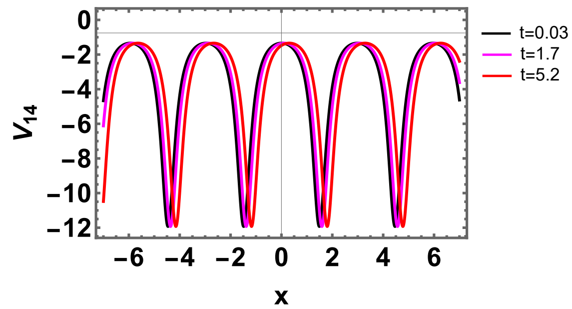

(f) Two dimensional plot (Imaginary part)

Figure 8. Plots to solution (3.48).

Remark: The wave profiles of $U(x,t)$ can be determined by applying Eq (3.5).

4. Interaction aspects

In this section, I present several dynamical wave phenomena utilizing the logarithmic transformation $\Phi = (\ln f)_\zeta$ [39]. Thus, substituting this transformation into Eq (3.6) yields

$$\left(f_\zeta\right)^3\left(a(b+2c)+12dr^2s\right)+6f^2s\left(dr^2f_{\zeta\zeta\zeta}-sf_\zeta\right)-18dfr^2sf_{\zeta\zeta}f_\zeta=0. \tag{4.1}$$

4.1. Multi-wave hypotheses

The multi-wave solutions [40] for Eq (4.1) can be obtained with the application of the following test function:

$$f = \kappa_2 \cosh(\delta_6 + \delta_5\zeta) + \kappa_1 \cos(\delta_4 + \delta_3\zeta) + \kappa_0 \cosh(\delta_2 + \delta_1\zeta), \tag{4.2}$$

where $\delta_n, n = 1, 2, \cdots, 6$ are constants. Equating coefficients for corresponding powers of hyperbolic and trigonometric functions to zero while solving Eqs (4.1) and (4.2) yields a system of equations. By employing computational tools like Mathematica, we resolve the system of equations and obtain the resulting solution sets as follows:

Set 1. When $\kappa_1 = 0,\ \delta_1 = -\delta_5,\ c = \frac{6s^2 - ab\delta_5^2}{2a\delta_5^2},\ d = -\frac{s}{2\delta_5^2 r^2}$, Eq (4.2) provides

$$f = \kappa_0 \cosh(\delta_2 - \delta_5\zeta) + \kappa_2 \cosh(\delta_5\zeta + \delta_6). \tag{4.3}$$

Thus,

$$\Phi = \frac{\delta_5\kappa_2 \sinh(\delta_5\zeta + \delta_6) - \delta_5\kappa_0 \sinh(\delta_2 - \delta_5\zeta)}{\kappa_0 \cosh(\delta_2 - \delta_5\zeta) + \kappa_2 \cosh(\delta_5\zeta + \delta_6)}. \tag{4.4}$$

Then, using Eq (4.4), the solution for Eq (2.1) is

$$V_1(x,t) = \frac{\delta_5 (\kappa_2 \sinh(\delta_6 + \delta_5 r(x - st)) - \kappa_0 \sinh(\delta_2 + \delta_5 r(st - x)))}{\kappa_0 \cosh(\delta_2 + \delta_5 r(st - x)) + \kappa_2 \cosh(\delta_6 + \delta_5 r(x - st))}. \tag{4.5}$$

Set 2. When $\delta_1 = \frac{\sqrt{s}}{\sqrt{-2dr}},\ \delta_5 = -\frac{\sqrt{s}}{\sqrt{-2dr}},\ \delta_3 = \frac{\sqrt{s}}{\sqrt{2}\sqrt{dr}}$, and $c = \frac{-ab - 12dr^2 s}{2a}$, Eq (4.2) results in

$$f = \kappa_1 \cos\left(\frac{\zeta\sqrt{s}}{\sqrt{2}\sqrt{dr}} + \delta_4\right) + \kappa_0 \cosh\left(\frac{\zeta\sqrt{s}}{\sqrt{2}\sqrt{-dr}} + \delta_2\right) + \kappa_2 \cosh\left(\frac{\zeta\sqrt{s}}{\sqrt{2}\sqrt{-dr}} - \delta_6\right). \tag{4.6}$$

Thus,

$$\Phi = \frac{-\frac{\kappa_1\sqrt{s}\sin\left(\frac{\zeta\sqrt{s}}{\sqrt{2}\sqrt{dr}} + \delta_4\right)}{\sqrt{2}\sqrt{dr}} + \frac{\kappa_0\sqrt{s}\sinh\left(\frac{\zeta\sqrt{s}}{\sqrt{2}\sqrt{-dr}} + \delta_2\right)}{\sqrt{2}\sqrt{-dr}} + \frac{\kappa_2\sqrt{s}\sinh\left(\frac{\zeta\sqrt{s}}{\sqrt{2}\sqrt{-dr}} - \delta_6\right)}{\sqrt{2}\sqrt{-dr}}}{\kappa_1 \cos\left(\frac{\zeta\sqrt{s}}{\sqrt{2}\sqrt{dr}} + \delta_4\right) + \kappa_0 \cosh\left(\frac{\zeta\sqrt{s}}{\sqrt{2}\sqrt{-dr}} + \delta_2\right) + \kappa_2 \cosh\left(\frac{\zeta\sqrt{s}}{\sqrt{2}\sqrt{-dr}} - \delta_6\right)}. \tag{4.7}$$

Then, we get the solution for Eq (2.1) using Eq (4.7) such as

$$V_2(x,t) = \frac{\sqrt{s}\left(\sqrt{d}\left(\kappa_0 \sinh\left(\frac{\sqrt{s}(x-st)}{\sqrt{2}\sqrt{-d}} + \delta_2\right) + \kappa_2 \sinh\left(\frac{\sqrt{s}(x-st)}{\sqrt{2}\sqrt{-d}} - \delta_6\right)\right) - \sqrt{-d}\kappa_1 \sin\left(\frac{\sqrt{s}(x-st)}{\sqrt{2}\sqrt{d}} + \delta_4\right)\right)}{\sqrt{2}\sqrt{-d^2}r\left(\kappa_1 \cos\left(\frac{\sqrt{s}(x-st)}{\sqrt{2}\sqrt{d}} + \delta_4\right) + \kappa_0 \cosh\left(\frac{\sqrt{s}(x-st)}{\sqrt{2}\sqrt{-d}} + \delta_2\right) + \kappa_2 \cosh\left(\frac{\sqrt{s}(x-st)}{\sqrt{2}\sqrt{-d}} - \delta_6\right)\right)}. \tag{4.8}$$

4.2. Homoclinic breather approach

Let the test function be defined as follows [40]:

$$f = \kappa_2 \cos(\nu(\delta_5\zeta + \delta_6)) + \kappa_1 \exp(\nu(\delta_3\zeta + \delta_4)) + \exp(-\nu(\delta_1\xi + \delta_2)), \tag{4.9}$$

where $\delta_l, l = 1, 2, \cdots, 6$ are constants. Substituting Eq (4.9) into Eq (4.1) yields the subsequent cases.

Set 1. When $\delta_1 = -i\delta_5,\ \delta_3 = -i\delta_5,\ s = 2d\delta_5^2\nu^2r^2$, and $c = \frac{-ab-24d^2\delta_5^2\nu^2r^4}{2a}$, Eq (4.9) gives that

$$f = \kappa_1 e^{\nu(\delta_4 - i\delta_5\zeta)} + \kappa_2 \cos(\nu(\delta_5\zeta + \delta_6)) + e^{-\nu(\delta_2 - i\delta_5\zeta)}. \tag{4.10}$$

Thus,

$$\Phi = -\frac{i\delta_5\nu\left(\kappa_1 e^{\nu(-2i\delta_5\zeta+\delta_2+\delta_4)} - i\kappa_2 e^{\nu(\delta_2-i\delta_5\zeta)}\sin(\nu(\delta_5\zeta+\delta_6)) - 1\right)}{\kappa_1 e^{\nu(-2i\delta_5\zeta+\delta_2+\delta_4)} + \kappa_2 e^{\nu(\delta_2-i\delta_5\zeta)}\cos(\nu(\delta_5\zeta+\delta_6)) + 1}. \tag{4.11}$$

Subsequently, Eq (4.11) presents the solution to Eq (2.1) as follows:

$$V_3(x,t) = -\frac{i\delta_5\nu\left(\kappa_1 e^{B\nu} - i\kappa_2 e^{\nu\left(2id\delta_5^3\nu^2r^3t+\delta_2-i\delta_5 rx\right)}\sin\left(\nu\left(-2d\delta_5^3\nu^2r^3t+\delta_6+\delta_5 rx\right)\right) - 1\right)}{\kappa_1 e^{B\nu} + \kappa_2 e^{\nu\left(2id\delta_5^3\nu^2r^3t+\delta_2-i\delta_5 rx\right)}\cos\left(\nu\left(-2d\delta_5^3\nu^2r^3t+\delta_6+\delta_5 rx\right)\right) + 1}, \tag{4.12}$$

where $B = 4id\delta_5^3\nu^2r^3t + \delta_2 + \delta_4 - 2i\delta_5 rx$.

Set 2. When $\kappa_1 = 0,\ \delta_1 = -i\delta_5,\ s = 2d\delta_5^2\nu^2r^2,\ c = \frac{-ab-24d^2\delta_5^2\nu^2r^4}{2a}$, Eq (4.9) results in

$$f = \kappa_2 \cos(\nu(\delta_5\zeta + \delta_6)) + e^{-\nu(\delta_2 - i\delta_5\zeta)}. \tag{4.13}$$

Thus,

$$\Phi = \frac{-\delta_5\kappa_2\nu\sin(\nu(\delta_5\zeta+\delta_6)) + i\delta_5\nu e^{-\nu(\delta_2-i\delta_5\zeta)}}{\kappa_2\cos(\nu(\delta_5\zeta+\delta_6)) + e^{-\nu(\delta_2-i\delta_5\zeta)}}. \tag{4.14}$$

Subsequently, Eq (4.14) provides the solution to Eq (2.1), as shown below:

$$V_4(x,t) = -\frac{\delta_5\nu\left(\kappa_2\exp\left(\nu\left(\delta_2 - i\delta_5 r\left(x - 2d\delta_5^2\nu^2r^2t\right)\right)\right)\sin\left(\nu\left(-2d\delta_5^3\nu^2r^3t+\delta_6+\delta_5 rx\right)\right) - i\right)}{1 + \kappa_2\exp\left(\nu\left(\delta_2 - i\delta_5 r\left(x - 2d\delta_5^2\nu^2r^2t\right)\right)\right)\cos\left(\nu\left(-2d\delta_5^3\nu^2r^3t+\delta_6+\delta_5 rx\right)\right)}. \tag{4.15}$$

4.3. Mixed type solutions

Assume the test function for mixed type solutions [41] may be expressed as

$$f = \kappa_3\sin(\delta_4+\delta_3\zeta) + \kappa_4\sinh(\delta_6+\delta_5\zeta) + \kappa_1\exp(\delta_2+\delta_1\zeta) + \kappa_2\exp(-(\delta_2+\delta_1\zeta)), \tag{4.16}$$

where $\kappa_n,\ n = 1,2,3,4$ and $\delta_l,\ l = 1,2,\cdots,6$ are constants. By substituting Eq (4.16) into Eq (4.1), we get the following cases.

Set 1. When $\kappa_3 = 0,\ \delta_1 = \delta_5,\ c = \frac{6s^2-ab\delta_5^2}{2a\delta_5^2},\ d = -\frac{s}{2\delta_5^2r^2}$, Eq (4.16) implies that

$$f = \kappa_1 e^{\delta_5\zeta+\delta_2} + \kappa_2 e^{-\delta_5\zeta-\delta_2} + \kappa_4\sinh(\delta_5\zeta+\delta_6). \tag{4.17}$$

Thus,

$$\Phi = \frac{\delta_5\kappa_1 e^{\delta_5\zeta+\delta_2} - \delta_5\kappa_2 e^{-\delta_5\zeta-\delta_2} + \delta_5\kappa_4\cosh(\delta_5\zeta+\delta_6)}{\kappa_1 e^{\delta_5\zeta+\delta_2} + \kappa_2 e^{-\delta_5\zeta-\delta_2} + \kappa_4\sinh(\delta_5\zeta+\delta_6)}. \tag{4.18}$$

Subsequently, Eq (4.21) provides the solution to Eq (2.1), as shown below:

$$V_6(x,t) = \frac{\delta_5\left(-\kappa_2 + \kappa_1 e^{2(\delta_2+\delta_5 r(x-st))} + \kappa_4 e^{\delta_2+\delta_5 r(x-st)}\cosh\left(\delta_6+\delta_5 r(x-st)\right)\right)}{\kappa_2 + \kappa_1 e^{2(\delta_2+\delta_5 r(x-st))} + \kappa_4 e^{\delta_2+\delta_5 r(x-st)}\sinh\left(\delta_6+\delta_5 r(x-st)\right)}. \tag{4.19}$$

Set 2. When $\kappa_2 = 0,\ \kappa_1 = 0,\ s = \frac{-ab-2ac}{12dr^2},\ \delta_3 = -\frac{\sqrt{-ab-2ac}}{2\sqrt{6}dr^2},\ \delta_5 = -\frac{\sqrt{a}\sqrt{b+2c}}{2\sqrt{6}dr^2}$, Eq (4.16) results in

$$f = \kappa_3\left(-\sin\left(\frac{\zeta\sqrt{-ab-2ac}}{2\sqrt{6}dr^2} - \delta_4\right)\right) - \kappa_4\sinh\left(\frac{\sqrt{a}\zeta\sqrt{b+2c}}{2\sqrt{6}dr^2} - \delta_6\right). \tag{4.20}$$

Thus,

$$\Phi = \frac{-\frac{\kappa_3\sqrt{-ab-2ac}\cos\left(\frac{\zeta\sqrt{-ab-2ac}}{2\sqrt{6}dr^2}-\delta_4\right)}{2\sqrt{6}dr^2} - \frac{\sqrt{a}\kappa_4\sqrt{b+2c}\cosh\left(\frac{\sqrt{a}\zeta\sqrt{b+2c}}{2\sqrt{6}dr^2}-\delta_6\right)}{2\sqrt{6}dr^2}}{\kappa_3\left(-\sin\left(\frac{\zeta\sqrt{-ab-2ac}}{2\sqrt{6}dr^2} - \delta_4\right)\right) - \kappa_4\sinh\left(\frac{\sqrt{a}\zeta\sqrt{b+2c}}{2\sqrt{6}dr^2} - \delta_6\right)}. \tag{4.21}$$

Equation (4.21) then provides the solution to Eq (2.1) in the following way:

$$V_7(x,t) = \frac{\kappa_3\sqrt{-a(b+2c)}\cos\left(\frac{\sqrt{-a(b+2c)}\left(at(b+2c)+12dr^2x\right)}{24\sqrt{6}d^2r^3} - \delta_4\right) + \sqrt{a}\kappa_4\sqrt{b+2c}\cosh\left(\frac{\sqrt{a}\sqrt{b+2c}\left(at(b+2c)+12dr^2x\right)}{24\sqrt{6}d^2r^3} - \delta_6\right)}{2\sqrt{6}dr^2\left(\kappa_3\sin\left(\frac{\sqrt{-a(b+2c)}\left(at(b+2c)+12dr^2x\right)}{24\sqrt{6}d^2r^3} - \delta_4\right) + \kappa_4\sinh\left(\frac{\sqrt{a}\sqrt{b+2c}\left(at(b+2c)+12dr^2x\right)}{24\sqrt{6}d^2r^3} - \delta_6\right)\right)}. \tag{4.22}$$

4.4. Periodic cross kink solutions

The test function for periodic cross kink solutions is defined as follows [42]:

$$f = \kappa_2\cos\left(\delta_4+\delta_3\zeta\right) + \kappa_3\cosh\left(\delta_6+\delta_5\zeta\right) + \delta_7 + \kappa_1\exp\left(\delta_2+\delta_1\zeta\right) + \exp\left(-\left(\delta_2+\delta_1\zeta\right)\right), \tag{4.23}$$

where $\kappa_j,\ j = 1,2,3$, and $\delta_l,\ l = 1,2,\cdots,7$ are constants. We ensure the following conditions by inserting Eq (4.23) into Eq (4.1).

Set 1. When $\kappa_2 = 0,\ \delta_5 = \delta_1,\ \delta_7 = 0,\ c = \frac{6s^2-ab\delta_1^2}{2a\delta_1^2},\ d = -\frac{s}{2\delta_1^2 r^2}$, Eq (4.23) yields that

$$f = \kappa_1 e^{\delta_1\zeta+\delta_2} + \kappa_3\cosh\left(\delta_1\zeta+\delta_6\right) + e^{\delta_1(-\zeta)-\delta_2}. \tag{4.24}$$

Thus,

$$\Phi = \frac{\delta_1\left(\kappa_1 e^{2(\delta_1\xi+\delta_2)} + \kappa_3 e^{\delta_1\zeta+\delta_2}\sinh\left(\delta_1\zeta+\delta_6\right) - 1\right)}{\kappa_1 e^{2(\delta_1\zeta+\delta_2)} + \kappa_3 e^{\delta_1\zeta+\delta_2}\cosh\left(\delta_1\zeta+\delta_6\right) + 1}. \tag{4.25}$$

The solution to Eq (2.1) is provided by Eq (4.25), which follows

$$V_8(x,t) = \frac{\delta_1\left(\kappa_1 e^{2(\delta_2+\delta_1 r(x-st))} + \kappa_3 e^{\delta_2+\delta_1 r(x-st)}\sinh\left(\delta_6+\delta_1 r(x-st)\right) - 1\right)}{\kappa_1 e^{2(\delta_2+\delta_1 r(x-st))} + \kappa_3 e^{\delta_2+\delta_1 r(x-st)}\cosh\left(\delta_6+\delta_1 r(x-st)\right) + 1}. \tag{4.26}$$

4.4.1. Graphical representations of the obtained solutions with applications

Figure 9 shows the dynamical behavior solution (4.8) for the parametric values $\delta_2 = 0.56$, $\delta_4 = 0.16$, $\delta_6 = 0.06$, $d = 0.56$, $\kappa_0 = 0.09$, $\kappa_1 = 0.2$, $\kappa_2 = 0.22$, $r = 0.7$, and $s = 0.84$.

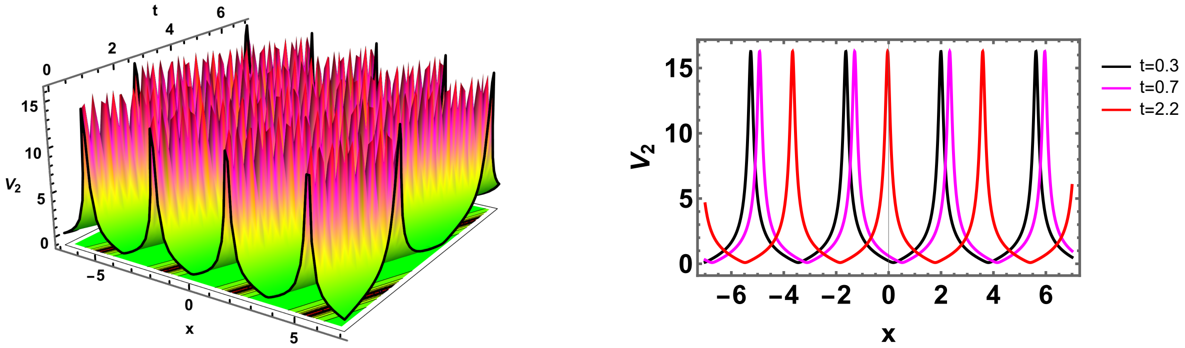

(a) Three dimensional and contour plots **(b)** Two dimensional plot

Figure 9. Plots to solution (4.8).

Multi-wave solutions in fluid dynamics are used to describe complicated interactions, such as collisions of waves and resonant waves, and predict extreme events and energy distribution in oceans and flow in the atmosphere accurately. Multi-wave superposition finds application in telecommunications in wavelength-division multiplexing and nonlinear signal processing, where it has been shown to greatly enhance bandwidth and data throughput in optical fiber networks. The stability criteria, phase-matching conditions, and the management of the interference that is needed to control the propagation of waves in nonlinear dispersive media are revealed through their analytical tractability. Multi-wave frameworks, therefore, play a central role in the future of predictive hydrodynamic modeling, as well as high-capacity communication technology with resiliency to interference. The dynamical behavior of the breather soliton (4.12) has been shown in Figure 10 with the values $d = 5.2$, $\delta_2 = 0.2$, $\kappa_1 = 0.5$, $\kappa_2 = 3.5$, $\nu = 0.1$, $r = 1.57$, $s = 0.94$, $\delta_4 = 2.22$, $\delta_5 = 3.2$, and $\delta_6 = 1.2$.

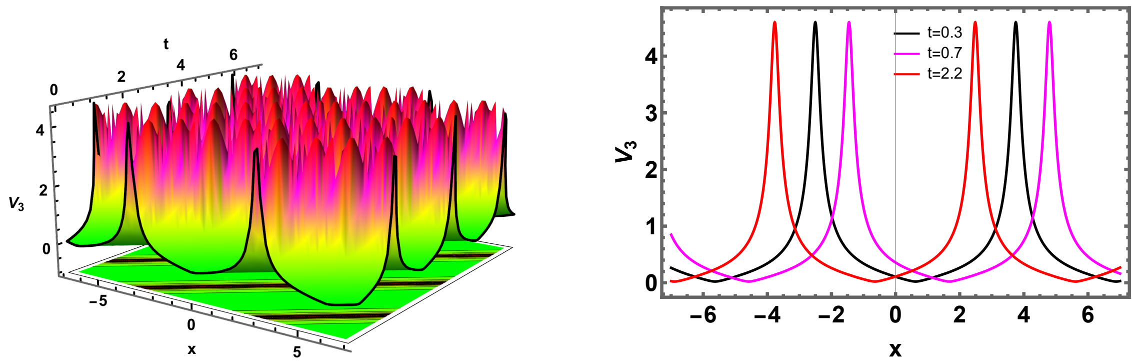

(a) Three dimensional and contour plots **(b)** Two dimensional plot

Figure 10. Plots to solution (4.12).

Breather solitons in fluid dynamics model pulsating wave packets that are a good predictor of the occurrence of rogue waves and energy concentration in oceans and stratified media. They are used in telecommunications to permit periodic pulse compression and stable signal regeneration in optical fibers to improve bandwidth efficiency and dispersion management. This oscillatory stability displays vital nonlinear energy-exchange processes and resonance limits that avoid disastrous wave breakdown and signal distortion. Therefore, breather solitons are indispensable to predicting extreme hydrodynamic hazards, and building self-governing photonic communication networks with high-resilience.

5. Conclusions

In this work, we have successfully applied several analytical methods, namely, the Kumar-Malik method, the generalized Arnous method, the RMESEM, and the logarithmic transformation to investigate soliton solutions of the coupled DSW system. Through this exploration, a diverse range of solution families has been derived, including periodic, bright, dark, kink, breather, multiwave, and exponential soliton solutions, which collectively provide deeper insight into the system's rich nonlinear dynamics. The validity of the obtained solutions has been confirmed through substitution into the original system. The 2D, 3D, and contour plots depict the effects of the physical parameters on the wave behavior and demonstrate the effectiveness of the methods used.

Based on these findings, several future research directions are proposed: (i) extending the methods to (2+1)- and (3+1)-dimensional nonlinear systems for more realistic physical modeling; (ii) applying more sophisticated analytical tools to uncover additional new soliton solutions; (iii) comparing the exact solutions obtained herein with numerical simulations and experimental data to validate their practical applicability; (iv) generalizing these approaches to fractional-order nonlinear systems to explore anomalous diffusion and memory effects; (v) further investigating multi-wave phenomena, including collision dynamics, fission-fusion processes, and their potential applications in optical switching and ocean wave energy harvesting.

In summary, I introduces a comprehensive analysis of soliton solutions and a multitude of potential directions for theoretical and applied future research in the field of nonlinear science.

Use of Generative-AI tools declaration

The author declares he has not used Artificial Intelligence (AI) tools in the creation of this article.

Conflict of interest

The author declares no conflict of interest in this paper.

References

1. Z. P. Yang, W. P. Zhong, M. Belić, Dark localized waves in shallow waters: analysis within an extended Boussinesq system, *Chinese Phys. Lett.*, **41** (2024), 044201. https://doi.org/10.1088/0256-307X/41/4/044201
2. A. Ahmed, A. R. Alharbi, H. S. Alayachi, I. Hashim, Exact and numerical approaches for solitary and periodic waves in a (2+1)-dimensional breaking soliton system with adaptive moving mesh, *AIMS Math.*, **10** (2025), 8252–8276. https://doi.org/10.3934/math.2025380

3. A. R. Alharbi, Traveling-wave and numerical solutions to nonlinear evolution equations via modern computational techniques, *AIMS Math.*, **9** (2024), 1323–1345. https://doi.org/10.3934/math.2024065
4. Y. Chen, Z. Y. Yan, H. Zhang, New explicit solitary wave solutions for (2+1)-dimensional Boussinesq equation and (3+1)-dimensional KP equation, *Phys. Lett. A*, **307** (2003), 107–113. https://doi.org/10.1016/S0375-9601(02)01668-7
5. X. Lü, F. H. Lin, Soliton excitations and shape-changing collisions in alpha helical proteins with interspine coupling at higher order, *Commun. Nonlinear Sci. Numer. Simul.*, **32** (2016), 241–261. https://doi.org/10.1016/j.cnsns.2015.08.008
6. T. G. Alharbi, A. Alharbi, Traveling-wave and numerical investigations to nonlinear equations via modern computational techniques, *AIMS Math.*, **9** (2024), 14310–14311. https://doi.org/10.3934/math.2024695
7. S. H. Alhejaili, H. S. Alayachi, F. A. H. Asiri, A. R. Alharbi, A. R. Seadawy, Analytical and numerical investigation of exact wave patterns and chaotic dynamics in the extended improved Boussinesq equation, *Open Phys.*, **23** (2025), 20250146. https://doi.org/10.1515/phys-2025-0146
8. G. Schneider, H. Uecker, *Nonlinear PDEs: A dynamical systems approach*, American Mathematical Society, 2017. https://doi.org/10.1090/gsm/182
9. J. L. Shen, J. Muhammad, U. Younas, Investigating the wave dynamics and interaction structures: exploring the Benney-Roskes/Zakharov-Rubenchik model in the oceanic atmosphere, *Ocean Eng.*, **354** (2026), 124969. https://doi.org/10.1016/j.oceaneng.2026.124969
10. U. Younas, A. R. Abdullah, F. P. Yao, J. Muhammad, Fractional longitudinal wave dynamics in magneto-electro-elastic materials: a neural network-based approach, *Fractal Fract.*, **10** (2026), 370. https://doi.org/10.3390/fractalfract10060370
11. A. Saleem, M. Abbas, M. A. El-Rahman, A. Birhanu, M. Z. Yousaf, H. Ahmad, Soliton solutions for the nonlinear Zoomeron equation applying the modified Khater method, *Sci. Rep.*, **16** (2026), 17355. http://doi.org/10.1038/s41598-026-55785-2
12. J. L. Shen, M. Liu, J. B. Liang, R. F. Zhang, New solutions to the (3+1)-dimensional HB equation using bilinear neural networks method and symbolic ansatz method using neural network architecture, *AIMS Math.*, **10** (2025), 30307–30330. http://doi.org/10.3934/math.20251331
13. X. Y. Chen, X. Yan, X. N. Zhang, F. Wang, T. Suzuki, Y. Ohishi, et al., Highly sensitive nonlinear temperature sensor based on soliton self-frequency shift technique in a microstructured optical fiber, *Sensors Actuators A Phys.*, **334** (2022), 113333. https://doi.org/10.1016/j.sna.2021.113333
14. E. M. E. Zayed, M. E. M. Alngar, R. M. A. Shohib, A. Biswas, Y. Yildirim, L. Moraru, et al., Highly dispersive solitons in optical couplers with metamaterials having Kerr law of nonlinear refractive index, *Ukr. J. Phys. Opt.*, **25** (2024), 01001–01019. https://doi.org/10.3116/16091833/Ukr.J.Phys.Opt.2024.01001
15. A. H. Arnous, Optical solitons with Biswas-Milovic equation in magneto-optic waveguide having Kudryashov's law of refractive index, *Optik*, **247** (2021), 167987. https://doi.org/10.1016/j.ijleo.2021.167987
16. J. L. Shen, R. F. Zhang, J. W. Huang, J. B. Liang, Neural network-based symbolic computation algorithm for solving (2+1)-dimensional Yu-Toda-Sasa-Fukuyama equation, *Mathematics*, **13** (2025), 3006. https://doi.org/10.3390/math13183006

17. J. L. Shen, X. Y. Wu, Periodic-soliton and periodic-type solutions of the (3+1)-dimensional Boiti-Leon-Manna-Pempinelli equation by using BNNM, *Nonlinear Dyn.*, **106** (2021), 831–840. https://doi.org/10.1007/s11071-021-06848-8
18. H. S. Alayachi, A. Alharbi, E. K. El-Shewy, M. A. E. Abdelrahman, New super and shock like solitary structures for KdV equation with higher-order nonlinearity, *Alex. Eng. J.*, **119** (2025), 503–510. https://doi.org/10.1016/j.aej.2025.01.124
19. A. Abdelrazec, D. Pelinovsky, Convergence of the Adomian decomposition method for initial-value problems, *Numer. Methods Partial Differ. Equ.*, **27** (2011), 749–766. https://doi.org/10.1002/num.20549
20. U. Younas, J. Muhammad, Q. Ali, M. Sediqmal, K. Kedzia, A. Z. Jan, On the study of solitary wave dynamics and interaction phenomena in the ultrasound imaging modelled by the fractional nonlinear system, *Sci. Rep.*, **14** (2024), 26080. https://doi.org/10.1038/s41598-024-75494-y
21. F. Javed, B. Rani, Y. Chahlaoui, H. M. Baskonus, N. Raza, Nonlinear dynamics of wave structures for the Davey-Stewartson system: a truncated Painlevé approach, *Nonlinear Dyn.*, **112** (2024), 22189–22200. https://doi.org/10.1007/s11071-024-10189-7
22. U. Younas, J. Muhammad, M. A. S. Murad, D. K. Almutairi, A. Khan, T. Abdeljawad, Investigating the truncated fractional telegraph equation in engineering: solitary wave solutions, chaotic and sensitivity analysis, *Results Eng.*, **25** (2025), 104489. https://doi.org/10.1016/j.rineng.2025.104489
23. E. M. E. Zayed, Y. A. Amer, R. M. A. Shohib, The improved generalized Riccati equation mapping method and its application for solving a nonlinear partial differential equation (PDE) describing the dynamics of ionic currents along microtubules, *Sci. Res. Essays*, **9** (2014), 238–248. https://doi.org/10.5897/SRE2013.5772
24. K. Hosseini, F. Samadani, D. Kumar, M. Faridi, New optical solitons of cubic-quartic nonlinear Schrödinger equation, *Optik*, **157** (2018), 1101–1105. https://doi.org/10.1016/j.ijleo.2017.11.124
25. M. Mañas, Darboux transformations for the nonlinear Schrödinger equations, *J. Phys. A Math. Gen.*, **29** (1996), 7721. https://doi.org/10.1088/0305-4470/29/23/029
26. Y. Y. Gu, B. X. Chen, F. Ye, N. Aminakbari, Soliton solutions of nonlinear Schrödinger equation with the variable coefficients under the influence of Woods-Saxon potential, *Results Phys.*, **42** (2022), 105979. https://doi.org/10.1016/j.rinp.2022.105979
27. T. Y. Han, Z. Li, C. Y. Li, Bifurcation analysis, stationary optical solitons and exact solutions for generalized nonlinear Schrödinger equation with nonlinear chromatic dispersion and quintuple power-law of refractive index in optical fibers, *Phys. A*, **615** (2023), 128599. https://doi.org/10.1016/j.physa.2023.128599
28. J. Muhammad, Q. Ali, U. Younas, On the analysis of optical pulses to the fractional extended nonlinear system with mechanism of third-order dispersion arising in fiber optics, *Opt. Quant. Electron.*, **56** (2024), 1168. https://doi.org/10.1007/s11082-024-07061-8
29. F. N. K. Sağlam, S. Malik, Various traveling wave solutions for (2+1)-dimensional extended Kadomtsev-Petviashvili equation using a newly created methodology, *Chaos Solitons Fract.*, **186** (2024), 115318. https://doi.org/10.1016/j.chaos.2024.115318
30. A. H. Arnous, Optical solitons to the cubic quartic Bragg gratings with anti-cubic nonlinearity using new approach, *Optik*, **251** (2022), 168356. https://doi.org/10.1016/j.ijleo.2021.168356

31. Y. L. Xiao, S. Barak, M. Hleili, K. Shah, Exploring the dynamical behaviour of optical solitons in integrable Kairat-II and Kairat-X equations, *Phys. Scr.*, **99** (2024), 095261. https://doi.org/10.1088/1402-4896/ad6e34
32. S. Ur-Rehman, J. Ahmad, Dynamics of optical and multiple lump solutions to fractional coupled nonlinear Schrödinger equation, *Opt. Quant. Electron.*, **54** (2022), 640. https://doi.org/10.1007/s11082-022-03961-9
33. V. G. Drinfeld, V. V. Sokolov, Equations of Korteweg-de Vries type, and simple Lie algebras, *Dokl. Akad. Nauk SSSR*, **258** (1981), 11–16.
34. G. Wilson, The affine Lie algebra $C_2^{(1)}$ and an equation of Hirota and Satsuma, *Phys. Lett. A*, **89** (1982), 332–334. https://doi.org/10.1016/0375-9601(82)90186-4
35. M. Arshad, A. R. Seadawy, D. C. Lu, J. Wang, Travelling wave solutions of Drinfel'd-Sokolov-Wilson, Whitham-Broer-Kaup and (2+1)-dimensional Broer-Kaup-Kupershmit equations and their applications, *Chinese J. Phys.*, **55** (2017), 780–797. https://doi.org/10.1016/j.cjph.2017.02.008
36. M. H. Bashar, S. M. Y. Arafat, S. M. R. Islam, M. M. Rahman, Wave solutions of the couple Drinfel'd-Sokolov-Wilson equation: new wave solutions and free parameters effect, *J. Ocean Eng. Sci.*, 2022, In press. https://doi.org/10.1016/j.joes.2022.05.003
37. A. K. M. K. S. Hossain, H. Akter, M. A. Akbar, Soliton solutions of DSW and Burgers equations by generalized (G'/G)-expansion method, *Opt. Quant. Electron.*, **56** (2024), 653. https://doi.org/10.1007/s11082-024-06319-5
38. N. M. A. Alsafri, Solitonic behaviors in the coupled Drinfeld-Sokolov-Wilson system with fractional dynamics, *AIMS Math.*, **10** (2025), 4747–4774. https://doi.org/10.3934/math.2025218
39. A. R. Seadawy, S. T. R. Rizvi, Nimra, A study of breather lump wave, rogue wave, periodic cross kink wave, multi-wave, M-shaped rational and their interactions for generalized nonlinear Schrödinger equation, *J. Nonlinear Opt. Phys. Mater.*, **33** (2024), 2350049. https://doi.org/10.1142/S0218863523500492
40. A. Yusuf, T. A. Sulaiman, M. Inc, M. Bayram, Breather wave, lump-periodic solutions and some other interaction phenomena to the Caudrey-Dodd-Gibbon equation, *Eur. Phys. J. Plus*, **135** (2020), 1–8. https://doi.org/10.1140/epjp/s13360-020-00566-7
41. H. C. Ma, C. Y. Zhang, A. P. Deng, New periodic wave, cross-kink wave, breather, and the interaction phenomenon for the (2+1)-dimensional Sharmo-Tasso-Olver equation, *Complexity*, **2020** (2020), 4270906. https://doi.org/10.1155/2020/4270906
42. A. Yusuf, T. A. Sulaiman, A. S. Alshomrani, D. Baleanu, Breather and lump-periodic wave solutions to a system of nonlinear wave model arising in fluid mechanics, *Nonlinear Dyn.*, **110** (2022), 3655–3669. https://doi.org/10.1007/s11071-022-07789-6

AIMS Press